Determination of W_{air} in high-energy electron beams using graphite detectors

Bourgouin, Alexandra; Cojocaru, Claudiu; Ross, Carl; McEwen, Malcolm

Publisher's version / Version de l'éditeur:
https://doi.org/10.1002/mp.13772
Medical Physics, 2019-09-28

Determination of W_{air} in high-energy electron beams using graphite detectors

Alexandra Bourgouin
Department of Physics, Carleton University, Ottawa, ON K1S 5B6, Canada
Ionizing Radiation Standards, National Research Council of Canada, Ottawa, ON K1A 0R6, Canada

Claudiu Cojocaru, Carl Ross, and Malcolm McEwen[a)]
Ionizing Radiation Standards, National Research Council of Canada, Ottawa, ON K1A 0R6, Canada

(Received 2 May 2019; revised 9 July 2019; accepted for publication 1 August 2019;
published xx xxxx xxxx)

Purpose: ICRU Report 90 on Key Data for Ionizing-Radiation Dosimetry: Measurement Standards and Applications (2014) has reaffirmed the recommended value of the mean energy required to create an ion pair in air, W_{air}, to be 33.97(12) eV. The report also indicates that this "constant" of radiation dosimetry is energy independent above 10 keV, since there is no theoretical or experimental evidence to the contrary. The goal of this investigation is to obtain additional experimental determinations of W_{air} in high energy beams and thus to verify the suggested energy independence.
Methods: W_{air} can be evaluated by combining ionometric and calorimetric measurements with a calculated ratio of the absorbed dose in the ion chamber air cavity and that of the calorimeter absorbing element. In this investigation, a graphite parallel plate chamber and a graphite calorimeter were used and the dose ratio was calculated using the EGSnrc Monte Carlo code. Measurements were made in electron beams from the NRC Vickers linear accelerator at two incident energies, 20 and 35 MeV. A range of average energies at the measurement point were obtained by inserting graphite plates in the primary beam.
Results: The average value of W_{air} obtained in this investigation is 33.85(18) eV which is consistent with the recommended value of 33.97(12) eV where the number in brackets represents the combined standard uncertainty of the value, referring to the corresponding last digits. The individual values of W_{air} do not show any statistically significant energy dependence.
Conclusion: The overall combined uncertainty of 0.5% meets the original target of the investigation. A larger-scale investigation, involving more individual energy points and a wider range of electron energies is required to go further and, for example, comment on the W_{air} energy dependency question raised by Tessier *et al.* [Med. Phys. 2018;**45**:370–381]. [https://doi.org/10.1002/mp.13772]

Key words: average energy to create an ion pair in air, EGSnrc, graphite calorimeter, ionization chamber, megavoltage electrons beam, thermal simulation

1. INTRODUCTION AND PURPOSE

The International Commission on Radiation Units and Measurement (ICRU) carried out a critical review of the key data used for ionizing radiation dosimetry and summarized the results in ICRU Report 90.[1] This report has reaffirmed the accepted value of the mean energy expended by an electron, passing through dry air, to create an ion pair (W_{air}) to be 33.97(12) eV. Here, and throughout the text, the number in parentheses represents the standard uncertainty in the last digit. The report also indicates that this "constant" of radiation dosimetry does not depend on the incident beam energy above 10 keV, since there is no theoretical nor experimental evidence to the contrary. W_{air} has been extensively measured for low energy beams, under 1 MeV, for both photon and electron sources, but measurements with megavoltage beams are limited, with only one data set each published for high-energy electron and photon beams as shown in table 5.6 of ICRU report 90.[1] Cojocaru *et al.* reported a single value of W_{air} 33.84(14) eV in high-energy electron beams[2] (15 to 50 MeV) and Burns *et al.* obtained 34.03(7) eV in high-energy photon beams[3] (6 to 25 MV).

W_{air} is a key value in both air kerma standards and absorbed dose formalisms. It enters directly in the equation for air kerma,[4] but is only implicitly present in absorbed dose formalisms (e.g., AAPM TG-51[5] and IAEA TRS-398[6]). The k_Q (or k_{Q,Q_0}) approach in these protocols uses a conversion factor to transform an ionization chamber calibration coefficient obtained in one radiation quality (usually Co-60) for use in another. The calculation used to obtain these k_Q factors includes a ratio of W_{air} values for the two beams in question.

If W_{air} is constant for both the beam of quality Q and the reference beam Q_0, then the absorbed dose measured using a calibrated ion chamber does not depend on the absolute value of W_{air}. On the other hand, if W_{air} does depend on the beam quality, the variation of W_{air} may impact the absorbed dose to

water measurement accuracy, depending on the method used to obtain the k_Q factor. While a measured k_Q would directly take account of any W_{air} energy dependency, a calculated k_Q[7,8] factor would not *unless explicitly included*. The addendum to TG-51 (2014)[9] uses Monte Carlo-calculated k_Q factors and includes the assumption that W_{air} has no energy dependency above 10 keV. This is a simplification that is often missed in comparing dosimetry protocols, or comparing measured and calculated k_Q factors.

Andreo *et al.*[6] included an uncertainty component for the potential variation in W_{air} but had limited data on which to base an analysis. Muir *et al.*[8] published a comparison of consistent measured and calculated k_Q data sets and suggested a possible variation of W_{air} of up to 0.42 % for a 25 MV photon beam compared to the reference Co-60 beam. A recent re-analysis by Tessier *et al.*[10] of measured calorimeter to ion chamber ratios obtained in high-energy electron beams by Domen and Lamperti[11] has shown a possible energy dependence of W_{air} and an extreme interpretation of that data set would suggest a variation of up to 2% in the clinical energy range (although the physical basis for such a large variation is unclear). The present work aims to determine the absolute value of W_{air} in high-energy electron beams and to investigate the assumption that W_{air} is energy independent in the clinical range.

2. MATERIALS AND METHODS

The mean energy expended by a charged particle to create an ion pair, W_{air}, is defined as the total number of ion pairs created in an air volume by a charged particle that expends all its kinetic energy in the volume.[12] This investigation considers incident energies in the few tens of MeV and the average range in air of an electron with a kinetic energy of 35 MeV is above 100 m. Thus measuring W_{air} in a high energy beam, according to its definition, would require an impractical air volume. The differential form of W_{air}, w_{air}, is more suitable for measurement in this context. It should be noted that if W_{air} is indeed energy independent above 10 keV, then W_{air} and its differential form would be equal for electron energies well above 10 keV. By convention, and since the absolute value of W_{air} would be theoretically the same as w_{air} in the range investigated, the term W_{air} will be used in this paper.

The equation for the absorbed dose to an air cavity can be rewritten as:

$$W_{air} = \frac{D_{air}}{Q_{air}/m_{air}} = \frac{D_{med}}{Q_{air}/m_{air}} \left(\frac{D_{air}}{D_{med}}\right)_{MC} \quad (1)$$

where $Q_{air}[\mathrm{C}]$ is the ionization in the sensitive volume, $m_{air}[\mathrm{kg}]$ is the mass of air in that volume and $D_{air}\left[\mathrm{J\ kg^{-1}}\right]$ is the dose deposited in the volume. Using this equation W_{air} has the unit of J per C which is equivalent to eV per elementary charge. A direct measurement of the absorbed dose deposited in an air volume (ion chamber cavity), as indicated by the equation on the left is not practical, so the ionometric measurement is combined on the right with an absorbed dose to medium measurement, D_{med}, (e.g., via a calorimeter) and a dose ratio determined using a detailed Monte Carlo calculation. To minimize the sensitivity of the calculation to the geometry, it is preferable to use the same material for both detectors. Graphite has been selected for this investigation since it is solid, can be machined and the physical properties (thermal and radiation) required for this investigation are known.

2.A. Calorimetry, D_{med}

Graphite exposed to high-energy electron beams shows an insignificant heat defect[13] and there is no convective heat loss. The calorimetric absorbed dose equation can be written as:

$$D_{gr} = c_{gr} \cdot \Delta T \cdot k_{hc} \cdot k_{n-gr} \quad (2)$$

where c_{gr} is the specific heat capacity of graphite, ΔT is the temperature increase due to radiation, k_{hc} is the heat loss correction factor, and k_{n-gr} is a correction factor for nongraphite material within the calorimeter core, that is, the temperature sensor. The specific heat capacity of graphite has been measured at the National Physical Laboratory (NPL)[14] and the Bureau International des Poids et Mesures (BIPM)[15] giving a value of 709.6(1.1) J kg^{-1} K^{-1} and 710.1(5) J kg^{-1} K^{-1} at 22°C, respectively. In this investigation, the specific heat capacity has been taken to be the unweighted average of these published results, 709.9(5) J kg^{-1} K^{-1} at 22°C. The radiation perturbations from air gaps and dose profile correction factors[16] have been ignored since they will be implicitly included in the Monte Carlo dose ratio.

2.A.1. Detector design

The calorimeter used for this investigation is based on an open-to-atmosphere calorimeter design originally developed at the NPL[17] and is shown in Fig. 1. The calorimeter is operated at standard ambient pressure in a quasi-adiabatic mode, that is, there is no active control of the calorimeter core temperature and heat exchange between the calorimeter core and its surroundings is observed through heat loss after irradiation. The choice of this simple design was made after reviewing the literature which demonstrated that for high-energy electron beams with dose rates of 5 Gy/min or greater, the calorimeter could achieve a suitable level of precision and accuracy, comparable with more complex calorimeters using vacuum systems and active temperature control.[18]

The calorimeter graphite core is a disk of radius 10.803 (4) mm, thickness 2.692(1) mm and density 1.686(10) g/cm. The graphite core is enclosed in a graphite phantom, as shown in Fig. 1. The core is held in place by expanded polystyrene spacers of millimetric cube size. The graphite calorimeter core temperature sensors were two negative temperature coefficient (NTC) thermistor probes (Micro-Betachip GA10K3MCD1, Measurement Specialties, Boston, MA, USA) with a resistance of approximately 10 kΩ at 25°C. Each thermistor probe was embedded in a 0.7 mm^3 hole in the calorimeter core. The thermistor probes were connected to an AC Wheatstone bridge as shown schematically in

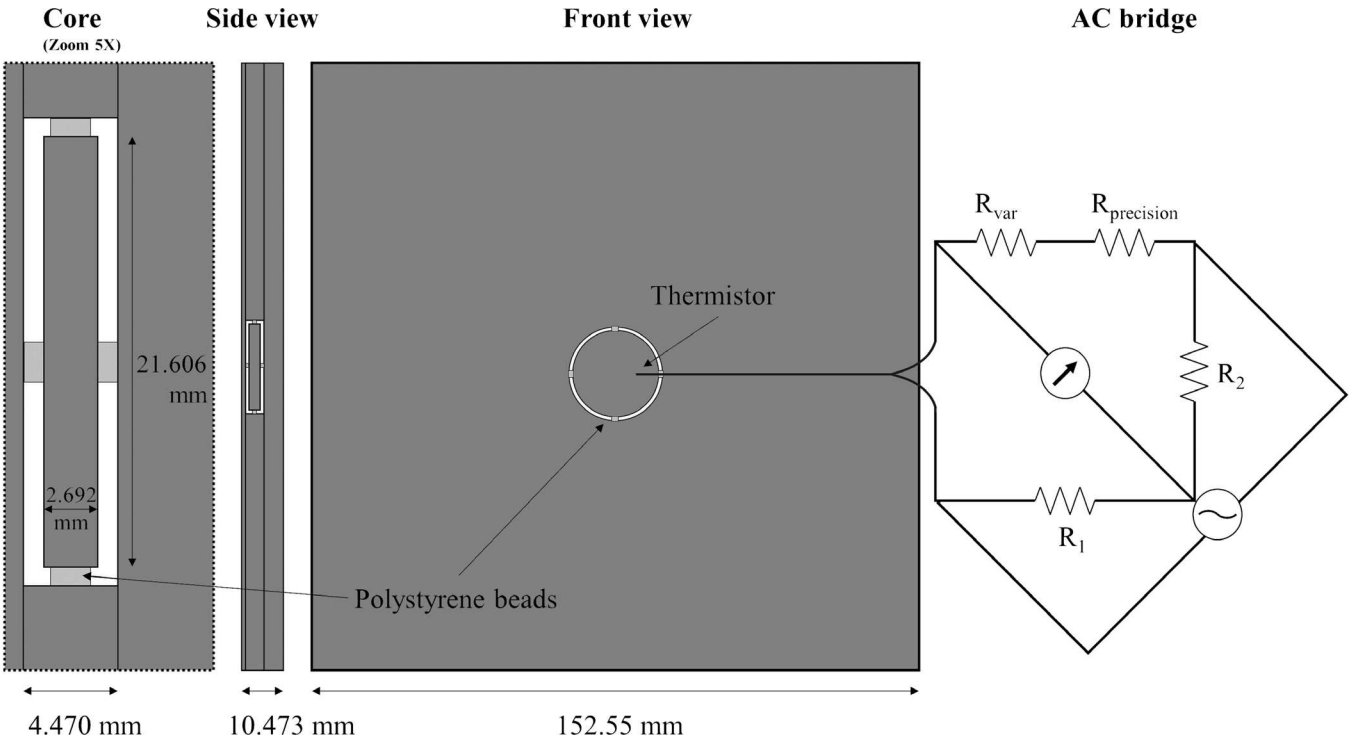

FIG. 1. Schematic of the graphite calorimeter detector and AC bridge. The drawing shows a single thermistor but two thermistors in series were actually used in this investigation. R_1, R_2, and $R_{precision}$ are fixed resistances of 10, 10, and 15 kΩ, respectively. R_{var} is a variable resistance used to balance the bridge.

Fig. 1. In practice, an active AC bridge as illustrated in Fig. 11 of McEwen and DuSautoy[19] was used. The dimensions of the thermistor probes are 0.5 mm diameter and a length of 3.3 mm which results in a k_{n-gr} correction of 1.0009. The calibration of the two thermistors has been made following the procedure described by Seuntjens *et al.*[20].

2.A.2. Temperature rise measurement, ΔT

The calorimetric measurement is performed in three phases, as shown in Fig. 2. The bridge output is measured for 30 s, which is called the preirradiation trace (from point A to B), to measure the background temperature drift. The calorimeter is then irradiated for a specific time (in this case 15 or 30 s, from points B to D). Once the beam is turned off, the bridge output is measured for 60 s to evaluate the postirradiation temperature drift (to point E). To extract the radiation-induced temperature rise, ΔT, from the temperature-time traces measured, the gradient (dT/dt) at points B and D has to be found and extrapolated to the mid-radiation (point C) as illustrated in Fig. 2(a). The gradient is usually taken to be the linear fit of the pre- and postirradiation trace for open-to-atmosphere graphite calorimetry,[21,22] which has shown agreement with other types of graphite calorimeter.[18,21] This extrapolation technique has been used to extract the radiation-induced temperature rise. As illustrated in Fig. 2(b), the ΔT calculated using this numerical approach is not sufficient to account for heat loss. The heat loss correction factors are calculated using thermal simulations and will be discussed in more detail in Section 2.E.

2.B. Ionometric measurement, Q_{air}/m_{air}

The corrected charge reading, Q_{air}, is found using the measured charge reading, Q_{raw}, and the following equation:

$$Q_{air} = Q_{raw} \cdot P_{TP} \cdot P_{ion} \cdot P_{pol} \cdot P_{elec} \cdot P_{leak} \cdot P_{rp} \cdot P_{SEE} \cdot k_{hum} \quad (3)$$

where the temperature-pressure correction factor, P_{TP}, has been applied to the charge measurement rather than the cavity mass. The ion recombination,P_{ion}, and polarity effect, P_{pol}, have been evaluated and will be discussed in more detail in Section 3.C. The electrometer calibration factor, P_{elec}, was measured using a charge-injection system[23] and found to be 1.0003(2). The leakage correction factor, P_{leak}, was also unity with negligible uncertainty since the average leakage current was below 0.005 % of the measured ionization chamber current during irradiation. The correction factor for the lateral variation of the beam intensity profile,P_{rp}, can be taken as unity because the effect of the beam profile is taken into account explicitly in the Monte Carlo dose ratio calculation. In addition, since the dimensions of the ion chamber and calorimeter core are very similar, there will be significant cancellation in any effect due to a nonflat lateral beam profile. The correction factor for humidity,k_{hum}, has also been included as W_{air} is defined for dry air (zero water vapor content). The value of k_{hum} is taken to be 0.9970.[24]

The correction factor, P_{SEE}, in Eq. (3) corrects for the effect of low-energy secondary electrons emitted from the graphite surfaces. This phenomenon is observed when the

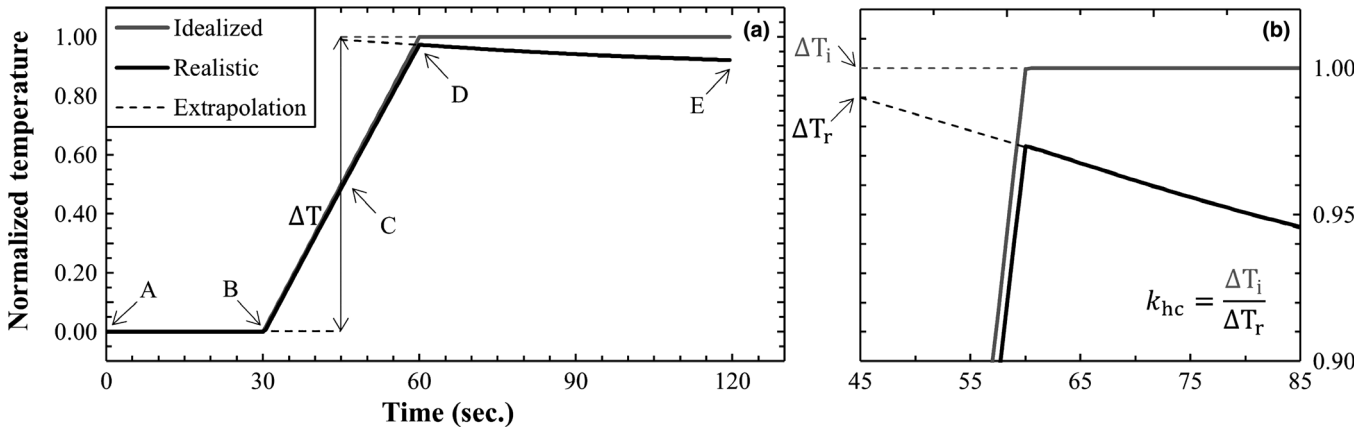

FIG. 2. Thermal simulation of calorimeter temperature-time traces representing typical measurement (realistic) and its associated ideal case where there is no heat loss. (b) Panel shows a zoom of (a) panel to illustrate the technique to extract the radiation induced temperature rise with the corresponding heat loss correction factor, k_{hc}.

air pressure in the ion chamber cavity is reduced to a negligible level but a nonzero ionization current is still recorded.[25] This effect has been reported previously and is consistent with secondary electron emission of low energy (under 50 eV) electrons from one electrode that would be collected due to the electric field, but do not have enough energy to ionize the air in the cavity. These electrons will contribute to the measured charge but do not contribute to energy deposition, and therefore a correction for them is required.

As the accuracy of the charge measurement obtained from the ionization chamber is crucial to the determination of W_{air}, some re-validation of the chamber's performance is required. The chamber has been used sporadically since the 1970s but no comprehensive testing has been carried out on it for some time. The chamber was therefore tested against the specification for a reference-class ion chamber given in the addendum to TG-51.[9]

2.B.1. Ion chamber design and charge measurement

The ion chamber used in this investigation is a graphite-walled symmetric plane parallel chamber, shown in Fig. 3, and is very similar to the one described by McCaffrey *et al.*[26] The ion chamber was built at the National Research Council of Canada (NRC) in 1973. The graphite rod used for machining the ion chamber pieces had a stated density of 1.706 (2) g/cm^3 (Ultra Carbon Corporation, Michigan, USA). The physical dimensions of the pieces surrounding the sensitive volume of the ion chamber had been measured prior to assembly and are listed in Table I.

This particular ion chamber has been selected for this investigation because of the distinctive features of having a design very similar to a calorimeter graphite core surrounded by a one millimeter air gap. The technical drawing of the ion chamber with the electrical connection is shown in Fig. 3.

2.B.2. Cavity mass, m_{air}

Evaluation of the air cavity mass, through volume and density is a crucial step in the determination of W_{air}. Any error in the evaluation of the sensitive volume of the ion chamber would lead to a systematic error in the absolute value of W_{air}. Using the mechanical dimensions of the ion chamber (the standard method used for primary standard Co-60 air kerma cavity chambers), the sensitive volume was found to be 0.8629(14) cm^3. The parallel-plate design of the chamber lends itself to an alternative route to determining the air volume, through a measurement of the capacitance. The advantage of this method is that it is carried out once the chamber is completely assembled and operational. The measurements were carried out in 1976, correcting for cable effects and the impact of the guard and collector not being perfectly planar (which modifies the electric field edge). The capacitance-based sensitive volume was found to be 0.86266 (21) cm^3, which is 0.03% lower than the mechanical measurement. Prior to using the chamber for this experiment, a series of QA tests were carried out, comparing the response of the chamber in Co-60 to other cavity ionization chambers with known volumes. These tests indicated that there was no change in the sensitive volume at the 0.1% level.

2.C. Radiation and detector phantom setup

Ionometric and calorimetric measurements have been performed using high-energy electron beams provided by the NRC Vickers linear accelerator, which have been characterized by Ross *et al.*[27] The energy spectrum at the linac exit window approximates a Gaussian shape with an uncertainty on the mean of 0.4 % and a sigma of 0.4%. The dose rate was 5 Gy/min for both incident energies used. A pure aluminum scattering plate was positioned at 3.5 cm from the linac exit window to spread the primary beam. The beam was then collimated using a standard clinical 6 cm × 6 cm applicator at 0.5 cm from the exit window, the scattering plate

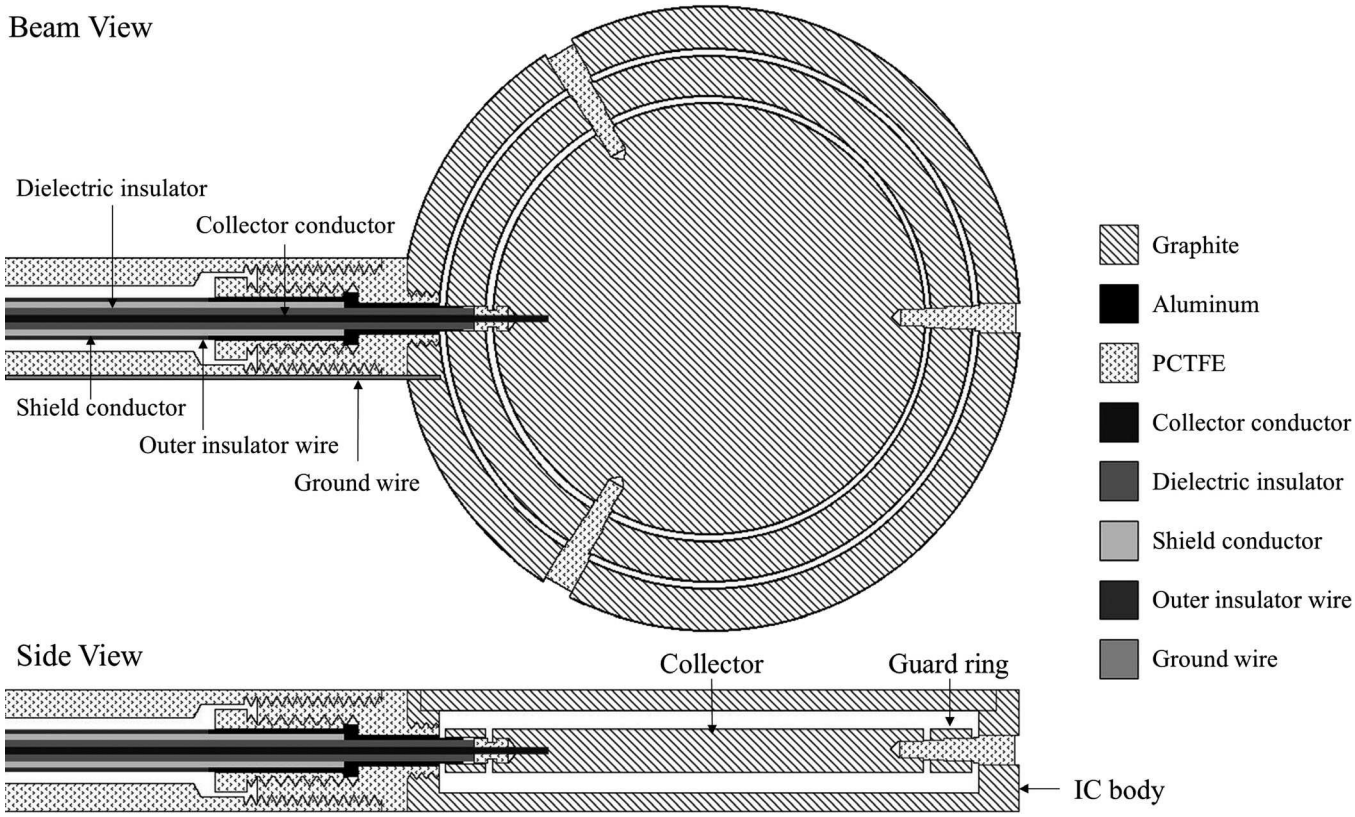

FIG. 3. Ion chamber technical drawing with its associated electrical connection using a coaxial cable and a ground wire.

being positioned between the first and second layers of the collimator (see Fig. 4). Two transmission chambers were installed after the electron applicator for beam monitoring and dose rate normalization purposes. The first was a PTW7862 chamber* and the second was an NRC-built device. The PTW chamber consists of four graphite-coated polyimide electrodes (28 mg/cm^2 in total) while the NRC chamber has two aluminum-coated polyethylene terephthalate electrodes and three gold-coated polyimide electrodes (56 mg/cm^2 in total). In addition, two Farmer-type field monitoring chambers were positioned at the edges of the primary beam in front of the detector phantom assembly, 1.5 m from the linac exit window. By monitoring the ratio of these two chamber readings it was possible to determine if there was any significant variation in the position of the beam.

Typical measurements consisted of a series of 10 measurements with each detector. To minimize the systematic effect of any drift in the linac output, the calorimeter and ion chamber were mounted on a translation stage and were alternated in the beam on a 5-minute cycle. Irradiation times for chamber and calorimeter were kept similar to avoid effects related to beam start-up.

The ion chamber and the calorimeter core were each enclosed in a graphite slab approximately 150 mm square to provide side and backscatter. A detailed list of graphite plates used in each detector's phantom is found in Table II. The graphite phantom was placed in an expanded polystyrene box to provide thermal isolation as shown in Fig. 5. It was not possible to use a phantom thickness adequate for full backscatter,[17] as this would have resulted in significant heat loss from the calorimeter due to the cold material behind.

TABLE I. Dimensions of the graphite components of the ion chamber used. Part labels are illustrated in Fig. 3.

Part name	Thickness (mm)	Diameter (mm)
IC collector	2.0117 (13)	21.57189 (32)
Guard ring	2.0134 (29)	O.D. 26.44572 (24) and I.D. 21.83155 (24)
Body	6.286 (77)	O.D. 30.937 (13) and I.D. 26.949 (13)
IC window	1.0092 (15)	28.964 (13)

The operational mode of the NRC Vickers linear accelerator meant that it was not straightforward to change the incident electron energy and therefore the electron energy at the point of interest (the air cavity of the ion chamber) was varied by changing the buildup thickness in front of the detector. It was possible to use two different linac energies, 20 and 35 MeV, and the buildup thicknesses were chosen to ensure an overlap in mean electron energy, at the point of interest, for two incident beam energies.

The radiation and buildup apparatus has been varied in terms of thermal and radiation conditions to investigate

*PTW Freiburg

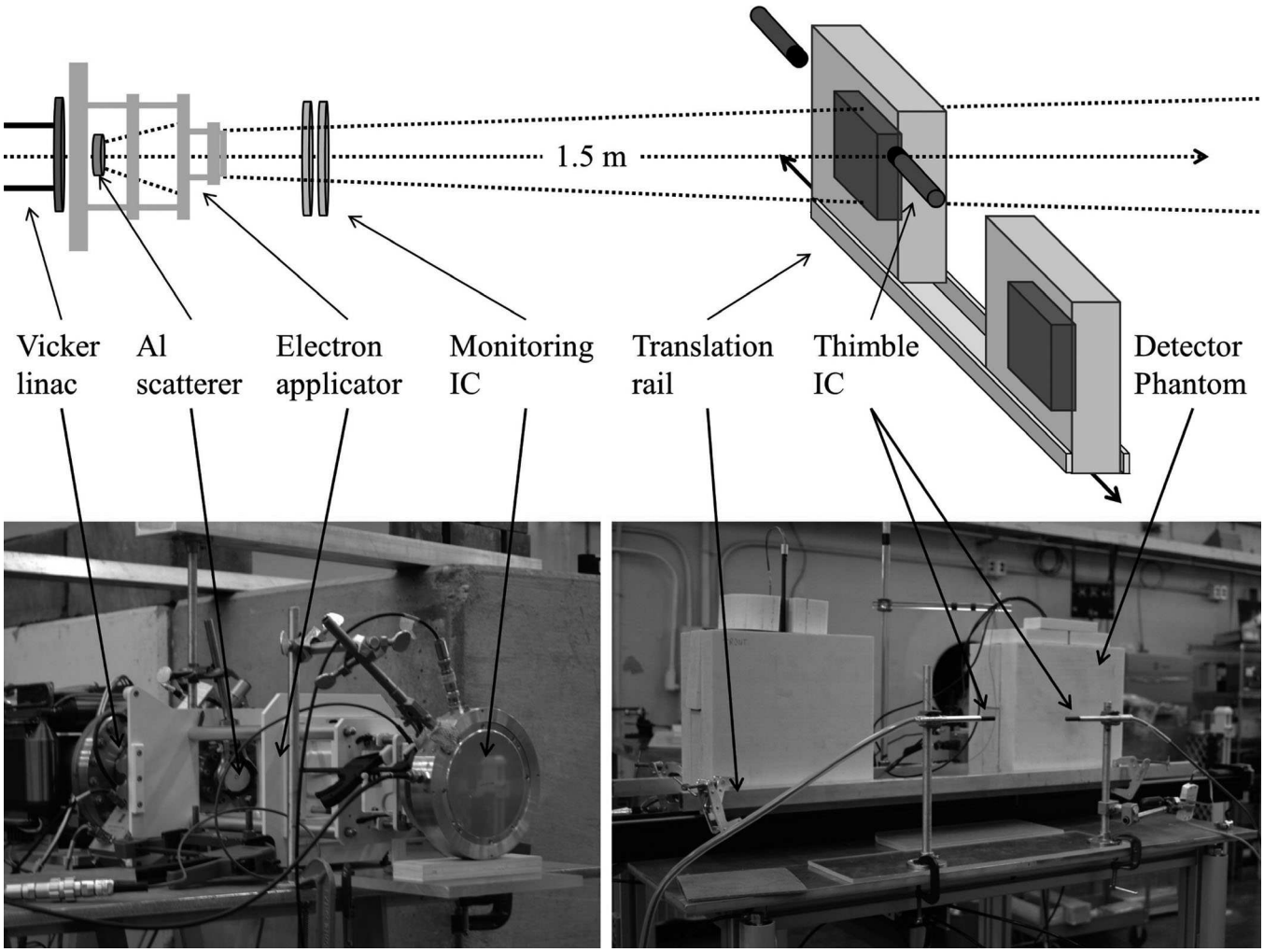

FIG. 4. Schematic radiation apparatus (upper drawing) with the detector phantom assembly and picture of the radiation setup (lower pictures).

possible systematic errors that could affect the analysis process through computer simulation (Monte Carlo or thermal simulation). To compare two similar radiation geometries but with a different thermal condition, the graphite buildup was positioned inside or outside (at 2.5 cm in front of phantom frame) of the insulating box as illustrated in Fig. 5. The irradiation time has also been varied to change the thermal environment without changing the experimental geometry. The radiation and thermal conditions used during this investigation are listed in Table III. The "null" listing in Table III indicates no additional buildup material, just the front plate of the calorimeter and ion chamber. The setup at 35 MeV with an inside buildup of 3.165 mm has been repeated over several days to verify reproducibility.

TABLE II. Mass thickness and thickness of graphite plates used for detector phantoms. Note that two plates were used for backscatter in the ion chamber phantom.

	Calorimeter		Ion chamber	
	Thickness (mm)	Mass thickness (g/cm^2)	Thickness (mm)	Mass thickness (g/cm^2)
Front plate	0.991 (11)	0.1761 (4)	0.998 (9)	0.1762 (18)
Sidescatter	4.740 (11)	0.8389 (139)	6.368 (25)	1.1228 (61)
Backscatter	4.741 (11)	0.8342 (74)	0.995 (9)	0.1757 (18)
			3.166 (12)	0.5866 (82)

2.D. Monte Carlo simulation

Monte Carlo dose calculations have been performed using the cavity application within the EGSnrc system[28] (released version 2017, commit 9266877). Electrons and photons have been tracked down to a kinetic energy of 1 keV. Range-based Russian roulette,[29] which is a well-known and tested variance reduction technique, has been used to increase the efficiency of the simulation. Custom density correction files have been generated for every graphite plate since the density of plates varied between 1.75 and 1.86 g/cm^3. The files have been created with the density effect parameter of the crystalline graphite form (density 2.265 g/cm^3, I_g = 81 eV) using ESTAR data[30] with the measured density in the header. Note that these are the values recommended by ICRU 90.[1]

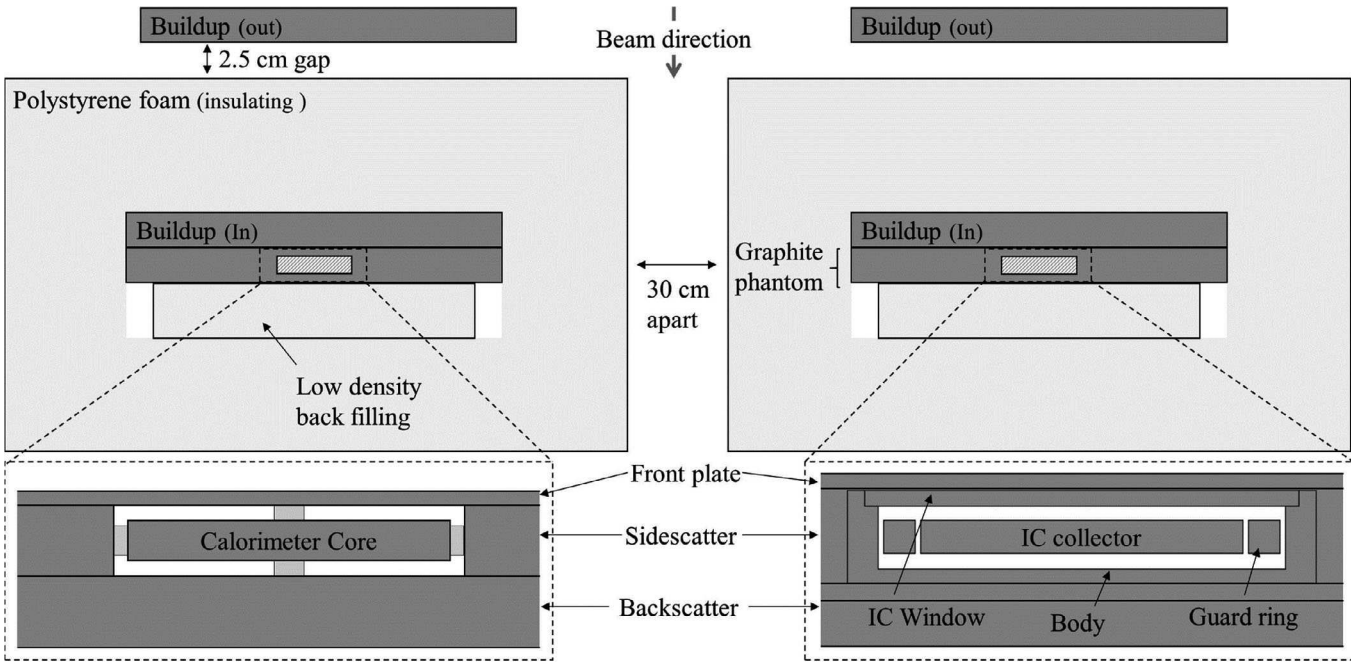

FIG. 5. Detector phantom assembly. The "back filling" is low density material to ensure good thermal contact between the graphite plates. Both buildup positions are illustrated, buildup "in" is positioned directly in front of the detector graphite phantom and the buildup "out" is positioned at 2.5 cm from the polystyrene box.

The beam source was simulated using `EGS_GaussianSpectrum Class Reference` with a mean energy of 20 or 35 MeV and a sigma of 0.4 %. The source was started outside the geometric domain with a circular beam of 0.01 cm radius and with an angular spread, sigma of 0.25°[27]. The geometry began with the 41.2 µm thick window of titanium alloy (Ti 90%, Al 6%, V 4%). The electron applicator was positioned at 5 mm in front of the exit window. The simulated electron applicator geometry consists of four layers of aluminum and lead in square shapes based on the measured dimensions of the one used. The pure aluminum scattering foil was positioned at 35 mm in front of the exit window, between the two first layers of the electron applicator, with a radius of 25 mm and a thickness of 4.0 or 7.0 mm depending on the beam energy (20 and 35 MeV respectively). The beam line simulation has been compared to a profile measurement using a Victoreen Thebes II Model 7020 ion chamber array. The detector geometry has been modeled following the details given above. The four monitoring ion chambers were not simulated since it was assumed they would not significantly perturb the radiation field. The Monte Carlo simulations have been tested using the recommended Fano test method,[31,32] which verifies the self-consistency of the transport algorithm. It also served as a verification of the calculated scoring volumes.

A sensitivity analysis of the Monte Carlo model was carried out by changing the mass thickness of graphite pieces within their own uncertainties (see Table III) and the mean energy of the beam within its estimated uncertainty, 0.4 %. For this sensitivity analysis the egs_chamber application within the EGSnrc system[28] was used. The type A (statistical) uncertainty limit was set to 0.1 % and electrons and photons were tracked down to a kinetic energy of 10 keV rather than 1 keV used for the "best" geometry. The use of a 10 keV cutoff significantly reduced the calculation time required, allowing a wider range of scenarios to be investigated.

TABLE III. Radiation and buildup apparatus variation. "Buildup position" refers to Fig. 5, whether it is positioned inside the detector phantom (In) or in front of the polystyrene box (Out).

Radiation			Buildup		
Energy (MeV)	Scatterer thickness (mm)	Radiation time (s)	Thickness (mm)	Mass thickness (g/cm^2)	Position (-)
20	4	15	Null	–	In
		30	Null	–	In
		15	9.513 (7)	1.7502 (3)	In
		30			In
		15	19.028 (11)	3.3453 (53)	In
		30			In
35	7	30	Null	–	In
		30	3.165 (4)	0.5869 (11)	In
		15	19.028 (11)	3.3453 (53)	In
		30			In
		15	38.056 (13)	6.6907 (74)	In
		30			In
		30	39.873 (14)	7.0754 (16)	Out

At the exit window of the beam line, before aluminum scatterer.

2.E. Thermal simulation

The heat loss correction factor, k_{hc}, is obtained using two simulated temperature-time traces, calculated by the finite-element method (FEM). The FEM software used in this investigation was COMSOL Multiphysics v.5.2. (COMSOL AB, Stockholm, Sweden). The realistic temperature-time traces were simulated by modeling the calorimeter and its immediate surrounding (graphite and expanded polystyrene phantom, see Fig. 5) in a 2D radial geometry. The heat source implemented was a dose deposition mapping obtained using the DOSXYZnrc application calculated for every radiation setup. To simulate the idealized temperature-time trace, the heat conductivity of the immediate medium surrounding the core was turned off. The heat loss correction factor is calculated using the same extrapolation technique for both thermal simulations as for the measured temperature-time traces. The heat loss correction factor is the ratio between the radiation temperature rise calculated for the idealized and realistic traces. The COMSOL simulations were compared to results obtained using FlexPDE, version 6 (PDE Solutions Inc., WA, USA). FlexPDE also uses the finite element method but the technique for describing the geometry, the differential equations and the boundary conditions is different from that of COMSOL.

3. RESULTS AND DISCUSSION

3.A. Monte Carlo

3.A.1. Results

Statistical (type A) uncertainties of 0.05% were obtained after typically 10^{10} histories for the ionometry dose calculation, and 0.04% after 10^9 histories for the calorimetry dose calculation. The electron spectra in the sensitive volume of the ion chamber were calculated using the cavity application, as shown in Fig. 6. At the incident beam energy of 20 MeV without buildup, the spectrum shows a double peak. This is due to the separation of the sensitive volume of the ion chamber by the collector as shown in Fig. 3. The double peak is not visible for other configurations due to broadening of the spectra.

3.A.2. Validation

Monte Carlo simulations have been run under Fano conditions for self-consistency testing. The dose scored in the regions of interest, the ion chamber air cavity and the calorimeter core, was within 0.06(3)% and 0.006(20)% of the theoretical Fano value, respectively. Over the entire geometry, the maximum deviation from the expected Fano value was 0.1%. The accuracy of the beam line simulation was tested by comparing the Monte Carlo-calculated beam profile to that measured using a linear array of 47 ion chambers (*Victoreen Thebes II Model 7020*) and the results are shown in Fig. 7.

As can be seen in Fig. 7, the measured profile is not symmetric, with the right side being slightly sharper then the left. This is consistent with the measurement of Ross *et al.*[27] and due to small asymmetries in the beam spot exiting the accelerator and minor deviations of the beam incident angle and position relative to the defined beam axis. Since the difference between simulated and measured profile within the dimension of the detector's sensitive volume (~1 cm radius) was smaller than the combined uncertainty, no modification was implemented in the beam simulated by Monte Carlo to account for this. As for the difference within the dimension of the graphite phantom (15 cm length), it was considered insignificant since the average difference was null. The right and left would balance in the thermal simulation input source.

The calculated Monte Carlo dose ratios have been compared to the restricted mass collision stopping power ratios calculated with the EGSnrc sprrznrc application, and the results are shown in Fig. 8. The energy variation of the stopping power ratio dominates the plot, as the other components of the dose ratio (ratio of perturbation factors for the ion chamber and calorimeter, backscatter differences, *etc*) are generally small at the energies investigated. As can be seen in Fig. 8(b), the product of these perturbation factors is of the order of 1.5%.

3.A.3. Sensitivity analysis

In Section 2.D, it was noted that a 10 keV cutoff was used for the sensitivity analysis simulations to reduce the calculation time. It was known that using a higher cutoff energy

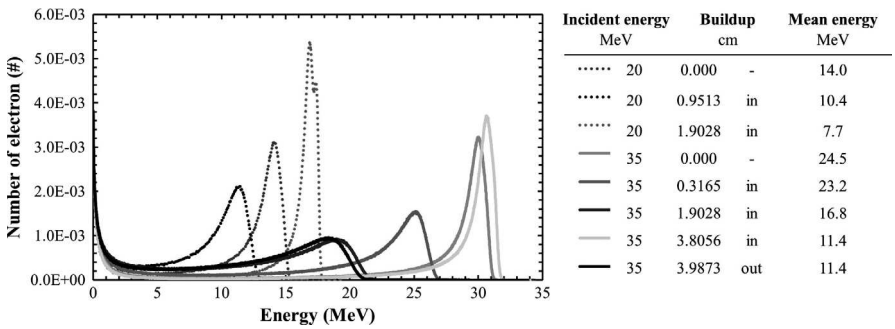

FIG. 6. Normalized electron energy spectra calculated by Monte Carlo using cavity application in the ion chamber sensitive volume for the different measurement configurations listed in Table III.

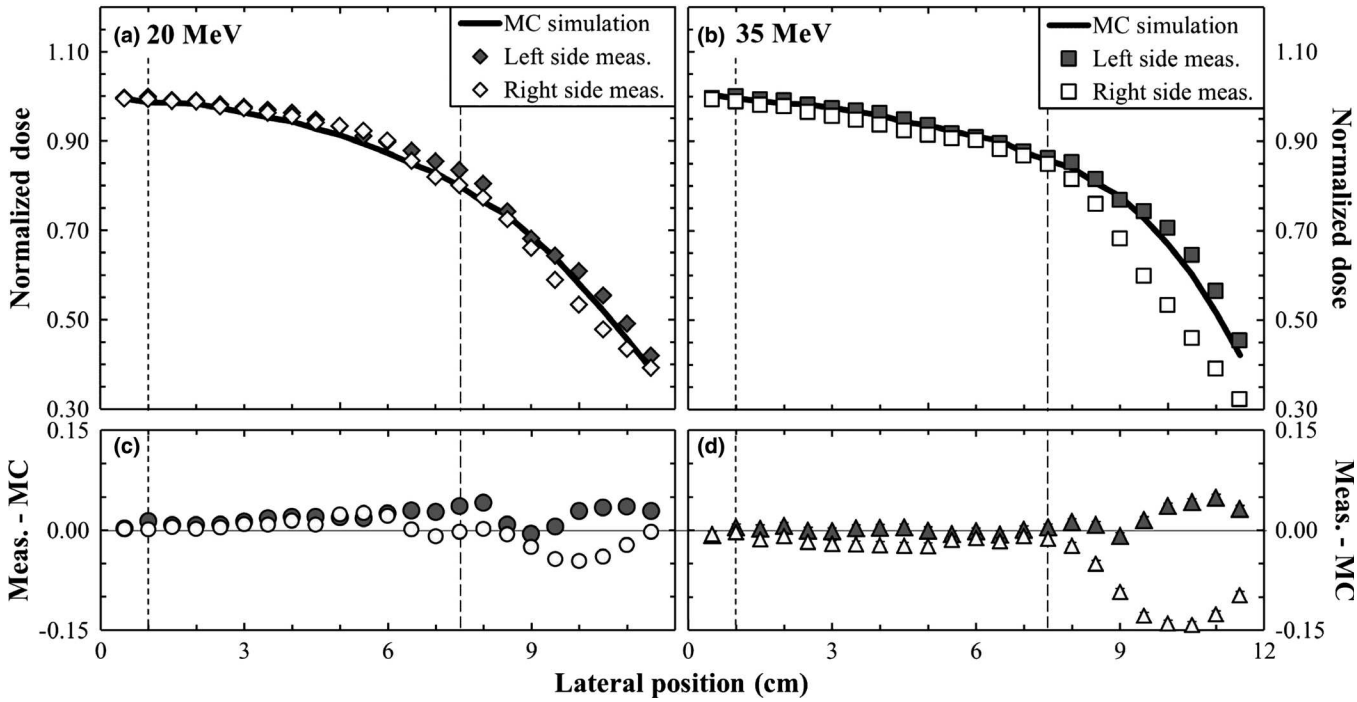

FIG. 7. Normalized 20 MeV (a) and 35 MeV (b) radial beam profiles measured and simulated at 1.5 m from the Vickers exit window and their relative difference: (c) 20 MeV, (d) 35 MeV. The vertical dashed lines represent the limit of the sensitive volume of the detectors and the limit of the graphite phantom, respectively.

would impact the absolute dose ratio (by up to 1%) but since the same cutoff was used in all scenarios investigated in the sensitivity analysis, any impact should cancel completely. The aim of this exercise was to investigate the relative impact of small changes in the mass thickness and/or incident electron energy.

Among all the different simulated scenarios, the largest deviation observed was 0.2%. In this particular case, the incident electron energy was at the limits of the specification, that is, ±0.4 %. The same deviation was also observed for a mass thickness at a value increased by the k = 1 uncertainty in the graphite density. In the other scenarios simulated, the deviation was within the statistical uncertainty of the simulation itself (0.1%).

3.B. Calorimetry: results and validation

Temperature-time traces of a measurement set are illustrated in Fig. 9(a) with its associated averaged traces compared to the thermal simulation in (b). In a perfectly controlled temperature environment, it would be expected to observe an increase in the postradiation trace curvature through successive measurements (a measurement set). However, the postradiation trace curvature, Fig. 9(a), has no distinctive trend and appears random. This is most likely due to the back-and-forth procedure swapping calorimeter and ion chamber in the beam.

The heat loss correction factor, k_{hc}, obtained for each radiation setup listed in Table III is shown in Fig. 10. The thermal model simulated was a single radiation run. It was decided to

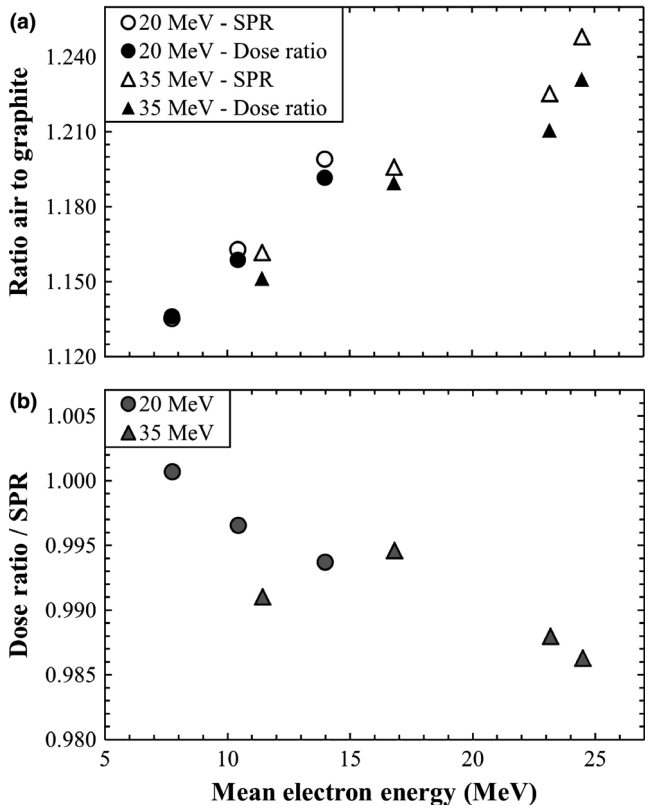

FIG. 8. (a) Monte Carlo dose ratio and stopping power ratio (SPR) of air with respect to graphite for the different irradiation conditions and (b) the ratio of the dose ratio to SPR.

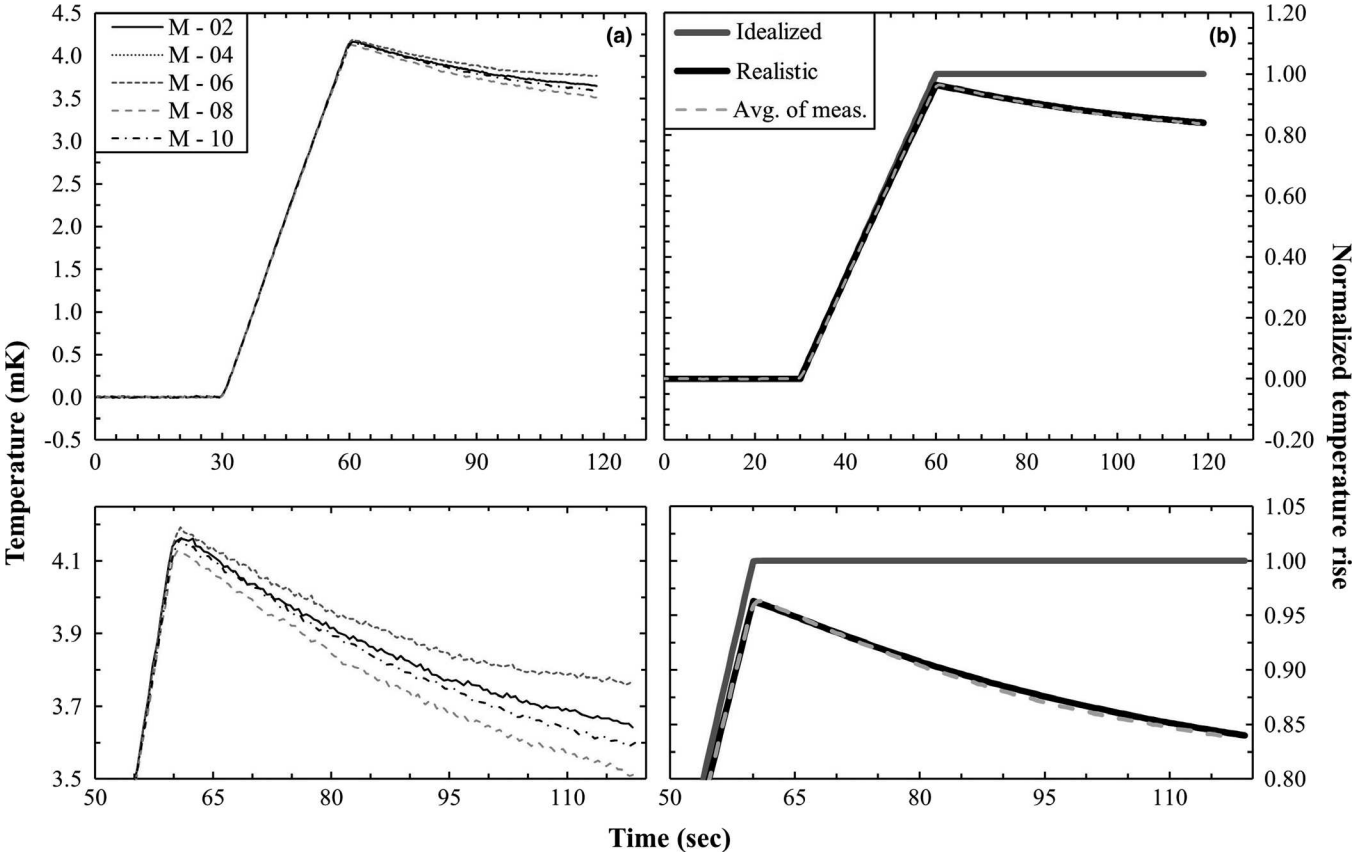

FIG. 9. A typical set of measured calorimeter temperature-time traces in (a), M-th represent the order in which the temperature-time trace has been measured and in (b), the corresponding normalized average compared to the simulated temperature-time trace.

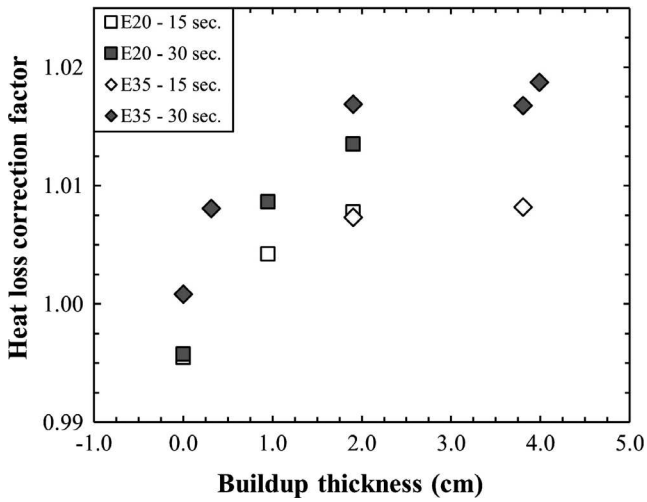

FIG. 10. Heat loss correction factor k_{hc} dependence on buildup thickness, irradiation time and primary beam energy; 20 MeV beam (E20) and 35 MeV beam (E35).

simulate it as a single run rather than a full simulation of the measurement (10 sets of irradiations with approximatively 10 min between each irradiation) due to the insufficient characterization of the thermal environment to correctly simulate it. Given the random distribution of postirradiation traces this approach is reasonable.

The heat loss correction factor increases with the thickness of the buildup material. This result was expected due to the increase in the nonuniformity of the dose deposition as a function of depth in the graphite phantom. The correction factor is also smaller for a shorter irradiation time since the heat loss rate is driven by the difference of the core temperature with it surrounding medium. It is larger for the 35 MeV beam compared to the 20 MeV beam, which is not expected since the depth-dose curves under 2 cm are very similar for both energies. This result shows the importance of the lateral dose uniformity in the graphite phantom. A 20 MeV beam scatters more in the lateral direction, provided better uniformity, compared to a 35 MeV beam. Also, the absolute dose deposition of the 20 MeV beam is smaller than the 35 MeV beam. This reduces the temperature difference between the graphite phantom and the polystyrene foam box in which the detector is placed. The uncertainty of the heat loss correction factor was evaluated for each measurement set and ranged from 0.04% to 0.79% with an average of 0.3%.

COMSOL and FlexPDE simulations of the heat-loss corrections agreed to within 0.07%, on average. The comparison is not a strict independent validation of the thermal model since both FEM simulations were based on the same input parameters, such as the energy deposition (from EGSnrc) and the material properties. However, the obtained consistency indicates no significant errors in coding the geometry or implementing the heat transfer equations.

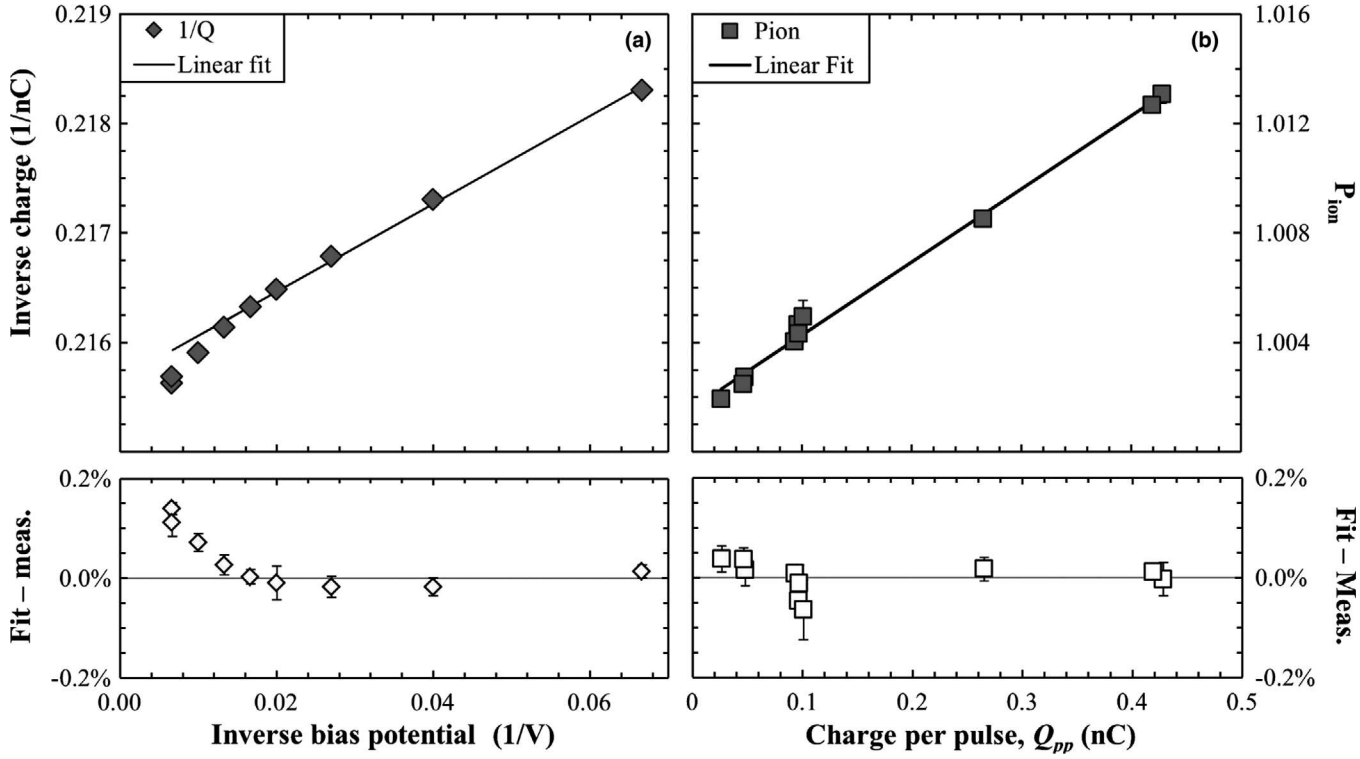

FIG. 11. The left-hand figure (a) shows an example of a JaffÉ plot obtained with the graphite parallel-plate ion chamber while the right-hand figure (b) shows the ion recombination correction factor as a function of the charge liberated per pulse, Q_{pp}, for an applied polarizing voltage of −75 V.

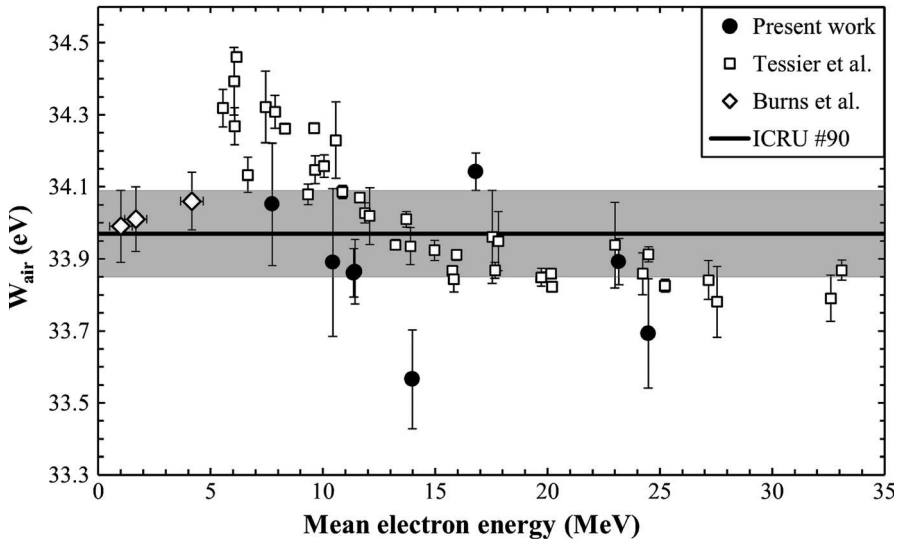

FIG. 12. The mean energy required to create ion pair in air, W_{air}, obtained in this investigation compared to the ICRU 90 recommendation, results of Tessier *et al.*[10] (Fig. 5) and Burns *et al.*[3] The uncertainty bars are only the Type A uncertainties (uncorrelated) for each measurement setup combined with heat loss correction uncertainty evaluated for each data set.

3.C. Ionometry; validation of reference-class behavior

The polarity effect was measured for each radiation setup listed in Table III. The smallest polarity correction was 1.0011 (1) and the largest one was 1.0034(2), a difference of 0.2%. A small dependency with energy has been observed, as expected due to the relatively thick collecting electrode in comparison with the electrode separation.[33,34] As mentioned in Section 2.B, the leakage has been measured to be 0.005% which is well below the 0.1% recommendation of the TG-51 addendum.[9]

The ion recombination correction has been measured in 8, 12, and 18 MeV beams from an Elekta Precise linac. An example of a Jaffé plot[35] obtained for a range of bias potentials between −15 and −150 V is shown in Fig. 11(a). As it

TABLE IV. Detailed W_{air} values obtained in this investigation. Single values are for each specific experiment with the combined standard uncertainties including both types A and B.

Incident energy (MeV)	Buildup (mm)	Mean energy in IC cavity (MeV)	Irradiation time (s)	W_{air} (eV)	W_{air} avg. (eV)
20	19.03	7.7	30	33.99 (19)	34.03 (19)
			15	34.07 (19)	
	9.51	10.4	30	33.85 (28)	33.87 (22)
			15	33.90 (16)	
	0.00	14.0	30	33.46 (22)	33.55 (17)
			15	33.64 (11)	
35	39.87	11.4	30	33.84 (11)	33.84 (11)
	38.06	11.4	30	33.81 (12)	33.85 (12)
			15	33.89 (13)	
	19.03	16.8	30	34.16 (10)	34.12 (10)
			15	34.09 (10)	
	3.17	23.2	30	33.87 (09)	33.87 (11)
			30	33.88 (12)	
			30	33.87 (11)	
	0.00	24.5	30	33.67 (17)	33.67 (17)
			Avg.	33.87 (15)	33.85 (18)

can be seen in the lower panel of Fig. 11(a), the inverse of charge collected is not linear at any potential applied, but the uncertainties of the linear fit is below the measurement uncertainties for a range from −15 to −75 V. Therefore, the bias potential applied on the ion chamber was selected to be −75 V.

The ion recombination correction factor should be linear with the charge created in the ion chamber cavity per linac output pulse, Q_{pp}, and the initial recombination should be less than 0.2%. To evaluate the initial recombination, the following equation[9] was used to fit the data shown in Fig. 11(b):

$$P_{ion} = 1 + C_{init} + C_{gen} \cdot Q_{pp} \tag{4}$$

where C_{init} accounts for initial recombination and C_{gen} is the coefficient of general (volume) recombination. The initial recombination, 0.160(17) %, is lower than the value specified in the TG-51 addendum and P_{ion} was linear with the dose per pulse as shown in Fig. 11(b).

The secondary electron emission correction, P_{SEE}, has been measured following the procedure of Bourgouin *et al.*[36] and has been found to be 0.9971(5) for beams of 12, 18, and 22 MeV from an Elekta Precise accelerator. No statistical difference has been measured between energies and so it is assumed that the same correction applies for the electron beams used here.

3.D. W_{air} results

The mean energy required to create an ion pair in air, W_{air}, obtained in this investigation is shown in Fig. 12 and in more detail in Table IV. The uncertainty bar in Fig. 12 is the type A standard uncertainty (k = 1) combined with the type B heat loss correction uncertainty evaluated for each measurement set. In Table IV, in the column 5, the uncertainty in the parentheses is the combined uncertainty (type A and B), which is detailed in Table V. In the last column, W_{air} has been averaged for every data set with the same energy at the point of measurement. In the last row, the average value for each column is presented. The value in parentheses of the last row, column 5, is the average uncertainty for each experiment and in column 6 is the standard deviation between experimental setups. The values of W_{air} obtained at different electron energies in this investigation are consistent with a constant value of 33.85(18) eV. The data obtained here do not show any significant trend with energy.

TABLE V. Relative standard uncertainties for the determination of W_{air} expressed in percent.

Component of Eq. (1)	Type A (%)	Type B (%)
D_{gr}		
Statistical standard deviation of ΔT	0.09	
Normalization ion chamber	0.06	
Specific heat capacity		0.07
Impurity correction factor		0.02
Thermistor calibration		0.05
Temperature extrapolation		0.25
Heat loss correction		0.31
Q_{air}/m_{air}		
Statistical standard deviation of Q_{raw}	0.02	
Normalization ion chamber	0.07	
Mass of air	0.02	0.10
Polarity effect	0.02	
Ion recombination		0.03
Secondary electrons emission	0.05	
Relative humidity		0.10
Monte Carlo dose ratio		
Statistical standard deviation	0.05	
Influence quantity (beam energy and mass thickness)		0.10
	0.15	0.43
Combined standard uncertainty	0.46	

Variation between setups ranged from 0.04% to 0.79%. Value in table represents the average. Specific value has been evaluated and applied in Table IV.

4. DISCUSSION

The average value obtained for W_{air}, 33.85(18) eV, is consistent with the recommended value of the ICRU 90, 33.97 (12) eV. This value agrees with the result of Burns *et al.*[3], 34.03(7) eV, in photon beams ranging from 6 to 25 MV using a similar approach. W_{air} obtained here is also consistent with the value of 33.84(14) eV reported by Cojocaru *et al.* in high-energy electron beams.[2] The data obtained are consistent with the hypothesis of the energy independency of W_{air}.

The data are self-consistent in that the standard deviation between experimental setups is 0.18 eV while the average uncertainty for each data set is approximately the same:

0.15 eV. Also, at the measurement point of around 11 MeV there is agreement where there is overlap between data obtained with the two incident energies of 20 and 35 MeV.

The uncertainty budget in Table V indicates that overall uncertainty is at the original target level of around 0.5% and that the majority of uncertainty components are under control. However, the investigation revealed that the simplicity of the open-to-atmosphere design of the calorimeter made the determination of the heat-flow correction rather challenging. It is recommended that for any future investigation, the calorimeter design should be revised to reduce the impact of the thermal simulation. An initial thermal simulation indicated that an improved geometry for the calorimeter core and air gap (e.g., improved mounting system for the core) can reduce the core-body heat transfer significantly.

The experiment is time-consuming (as with many calorimeter investigations) and so it was only possible to acquire a limited number of data points at different electron energies. It is recommended that any future investigation should focus on lower energies (in the range 6 to 10 MeV) and also higher energies (above 30 MeV) as this would provide data to comment more conclusively on the apparent energy dependence of W_{air} reported by Tessier *et al.*[10]

5. CONCLUSION

In this investigation, W_{air} was obtained using an open-to-atmosphere calorimeter with a graphite ion chamber combined with a Monte Carlo calculation of a dose ratio. Measurements were made in electron beams from a research linear accelerator at two incident energies, 20 and 35 MeV, with multiple energies at the measurement depth obtained by inserting graphite plates in the primary beam. A detailed Monte Carlo simulation of the complete experimental geometry was performed using the EGSnrc radiation transport system. A number of parallel investigations were carried out to validate the calorimeter and ion chamber performance and to characterize the sensitivity of the simulations.

No significant variation with energy was observed for W_{air} and the average value obtained for all radiation setups was 33.85(18) eV, which is 0.29% lower than the recommended value of 33.97(12) eV, but within the overall measurement uncertainties. The investigation highlighted that it would be useful to extend the measurements to cover a wider range of electron energies (particularly in the range 6 to 10 MeV) and that the calorimeter design could be improved to reduce the uncertainty in the correction for heat transfer.

ACKNOWLEDGMENTS

This research is supported in part by the Natural Sciences and Engineering Research Council of Canada (NSERC) doctoral scholarship program. The authors thank Frédéric Tessier for his help with EGSnrc simulation and for providing data for Fig. 12. The authors also thank Bill Henry and George Smith, now retired, for designing and building the ion chamber used in the work and for the detailed measurement of its volume.

CONFLICT OF INTEREST

The authors have no conflict to disclose.

[a]Author to whom correspondence should be addressed. Electronic mail: malcolm.mcewen@nrc-cnrc.gc.ca.

REFERENCES

1. ICRU. Key Data for Ionizing-Radiation Dosimetry: Measurement Standards and Applications. ICRU Rep 90 (International Comm Radiat Units Meas Bethesda, MD); 2014.
2. Cojocaru C, Ross C. Sci-Sat AM: brachy - 02: extracting W_{air} from the 1976 electron beam measurements of Domen and Lamperti. *Med Phys*. 2012;39:4645.
3. Burns DT, Picard S, Kessler C, Roger P. Use of the BIPM calorimetric and ionometric standards in megavoltage photon beams to determine W_{air} and I_c. *Phys Med Biol*. 2014;59:1353–1365.
4. AAPM TG-21 protocol for the determination of absorbed dose from high-energy photon and electron beams. *Med Phys*. 1983;10:741–771.
5. Almond PR, Biggs PJ, Coursey BM, et al. AAPM's TG-51 protocol for clinical reference dosimetry of high-energy photon and electron beams. *Med Phys*. 1999;26:1847–1870.
6. IAEA. Absorbed dose determination in external beam radiotherapy: an international code of practice for dosimetry based on standards of absorbed dose to water. Tech Rep TRS-398. IAEA, Vienna; 2000.
7. McEwen MR. Measurement of ionization chamber absorbed dose k_Q factors in megavoltage photon beams. *Med Phys*. 2010;37:2179–2193.
8. Muir BR, McEwen MR, Rogers DWO. Measured and Monte Carlo calculated k_Q factors: accuracy and comparison. *Med Phys*. 2011;38:4600–4609.
9. McEwen M, Dewerd L, Ibbott G, et al. Addendum to the AAPM's TG-51 protocol for clinical reference dosimetry of high-energy photon beams. *Med Phys*. 2014;41:041501.
10. Tessier F, Cojocaru CD, Ross CK. Extracting W_{air} from the electron beam measurements of Domen and Lamperti. *Med Phys*. 2018;45:370–381.
11. Domen S, Lamperti P. Comparisons of calorimetric and ionometric measurements in graphite irradiated with electrons from 15 to 50 MeV. *Med Phys*. 1976;3:294–301.
12. ICRU. International Commission on Radiation Units and Measurements. Average Energy Required to Produce an Ion Pair. ICRU Rep 31 (International Comm Radiat Units Meas. Bethesda, MD);1979.
13. Bewley DK, Page BC. Heat defect in carbon calorimeters for radiation dosimetry. *Phys Med Biol*. 1972;17:584.
14. Williams AJ, Burns DT, McEwen MR. Measurement of the specific heat capacity of the electron-beam graphite calorimeter. NPL Rep. Rep; 1993; NPL.
15. Picard S, Burns DT, Roger P. Determination of the specific heat capacity of a graphite sample using absolute and differential methods. *Metrologia*. 2007;44:294–302.
16. Seuntjens J, DuSautoy AR. Review of calorimeter based absorbed dose to water standards. In: Proceedings of International Symposium on Standards and Codes of Practice in Medical Radiation, Vienna, Nov. 2002. IAEA-CN-96-3; 2003;1:37–66.
17. McEwen MR, DuSautoy AR, Williams AJ. The calibration of therapy level electron beam ionization chambers in terms of absorbed dose to water. *Phys Med Biol*. 1998;43:2503–2519.
18. DuSautoy AR. The UK primary standard calorimeter for photon-beam absorbed dose measurement. *Phys Med Biol*. 1996;41:137–151.
19. McEwen MR, DuSautoy AR. Primary standards of absorbed dose for electron beams. *Metrologia*. 2009;46:S59–S79.
20. Seuntjens JP, Ross CK, Klassen N, Shortt KR. A status report on the NRC sealed water calorimeter. Ioniz Radiat Stand Inst Natl Meas Stand. Natl Res Counc Ottawa; 1999 (March).
21. Burns DT, Morris WT. A graphite calorimeter for electron beam dosimetry. High dose Dosim Radiat Process Proc. 1991;IAEA-SM-31: 123-136.

22. Renaud J, Marchington D, Seuntjens JP, Sarfehnia A. Development of a graphite probe calorimeter for absolute clinical dosimetry. *Med Phys*. 2013;40:020701.
23. Downton B, Walker S. Humidity effects on calibrations of radiation therapy electrometers. *Med Phys*. 2012;39:984–987.
24. Rogers DWO, Ross CK. The role of humidity and other correction factors in the AAPM TG-21 dosimetry protocol. *Med Phys*. 1988;15:40–48.
25. Wilson CW. Observations on the ionization produced by radium gamma rays in air-walled ionization chambers at low gas pressures. *Br J Radiol*. 1954;27:158–162.
26. McCaffrey JP, Mainegra-Hing E, Kawrakow I, Shortt KR, Rogers DWO. Evidence for using Monte Carlo calculated wall attenuation and scatter correction factors for three styles of graphite-walled ion chamber. *Phys Med Biol*. 2004;49:2491–2501.
27. Ross CK, McEwen MR, McDonald AF, Cojocaru CD, Faddegon BA. Measurement of multiple scattering of 13 and 20 MeV electrons by thin foils. *Med Phys*. 2008;35:4121–4131.
28. Kawrakow I, Mainegra-Hing E, Rogers DWO, Tessier F, Walters BRB. The EGSnrc Code System: Monte Carlo Simulation of Electron and Photon Transport; 2017. https://nrc-cnrc.github.io/EGSnrc/doc/pirs701-egsnrc.pdf
29. Fippel M.Variance reduction techniques. In: Seco J, Verhaegen F, eds. Monte Carlo Techniques in Radiation Therapy; 2013:29.
30. Berger MJ, Coursey JS, Zucker MA, Chang J. ESTAR, PSTAR, and ASTAR: Computer Programs for Calculating Stopping-Power and Range Tables for Electrons, Protons, and Helium Ions (version 1.2.3). National Institute of Standards and Technology, Gaithersburg, MD; 2005. http://physics.nist.gov/Star. Accessed June 12, 2017.
31. Kawrakow I. Accurate condensed history Monte Carlo simulation of electron transport. I. EGSnrc, the new EGS4 version. *Med Phys*. 2000;27:485–498.
32. Sempau J, Andreo P. Configuration of the electron transport algorithm of PENELOPE to simulate ion chambers. *Phys Med Biol*. 2006;51:3533–3548.
33. Burns DT, McEwen MR. Ion recombination corrections for the NACP parallel-plate chamber in a pulsed electron beam. *Phys Med Biol*. 1998;43:2033–2045.
34. Muir BR, McEwen MR, Rogers DWO. Beam quality conversion factors for parallel-plate ionization chambers in MV photon beams. *Med Phys*. 2012;39:1618–1631.
35. Jaffe G. On the theory of recombination. *Phys Rev*. 1940;58:968–976.
36. Alexandra Bourgouin MM. CIRMS 2017 Conference Gaithersburg, MD at NIST, March 27–29, 2017. In: Vacuum Current: A Possible Systematic Error in Absolute Dose/Kerma Measurements with Ion Chambers. Gaithersburg; 2017:28–29.